

SafeLink: Safety-Critical Control Under Dynamic and Irregular Unsafe Regions

Songqiao Hu, Zidong Wang, *Fellow, IEEE*, Zeyi Liu, Zhen Shen, and Xiao He, *Senior Member, IEEE*

Abstract—Control barrier functions (CBFs) provide a theoretical foundation for safety-critical control in robotic systems. However, most existing methods rely on explicit analytical expressions of unsafe state regions, which are often impractical for irregular and dynamic unsafe regions. This paper introduces SafeLink, a novel CBF construction method based on cost-sensitive incremental random vector functional-link (RVFL) neural networks. By designing a valid cost function, SafeLink assigns different sensitivities to safe and unsafe state points, thereby eliminating false negatives in classification of unsafe state points. Under the constructed CBF, theoretical guarantees are established regarding system safety and the Lipschitz continuity of the control inputs. Furthermore, incremental update theorems are provided, enabling precise real-time adaptation to changes in unsafe regions. An analytical expression for the gradient of SafeLink is also derived to facilitate control input computation. The proposed method is validated on the endpoint position control task of a nonlinear two-link manipulator. Experimental results demonstrate that the method effectively learns the unsafe regions and rapidly adapts as these regions change, achieving computational speeds significantly faster than baseline methods while ensuring the system safely reaches its target position.

Note to Practitioners—Ensuring the safety of multi-degree-of-freedom (DOF) robotic manipulators operating in unstructured environments remains a significant practical challenge. In real-world applications such as human-robot collaboration and warehouse automation, robots must avoid irregularly shaped and moving obstacles, including human operators, dynamic workpieces, stacked cargo, and temporarily restricted areas, whose precise mathematical representations are often unavailable. Traditional CBF-based control methods typically rely on explicit analytical models of such obstacles, which are difficult to construct and maintain in practice. The proposed SafeLink framework enables the controller to learn unsafe regions directly from sensor or user-provided data while maintaining conservative safety estimation and to update them online as the environment evolves. The approach enhances system safety while operating efficiently in real time, making it suitable for safety-critical robotic systems that require rapid adaptation to changing hazards.

Index Terms—Control barrier function, neural network, safety-critical control, learning for control, robotic manipulators.

This work was supported in part by National Natural Science Foundation of China under grants 62525308, 62473223, 52172323, and 624B2087, in part by Beijing Natural Science Foundation under grant L241016. (Corresponding author: Xiao He)

Songqiao Hu, Zeyi Liu and Xiao He are with the Department of Automation, and the Institute for Embodied Intelligence and Robotics, Tsinghua University, Beijing 100084, China (e-mails: hsq23@mails.tsinghua.edu.cn, liuzy21@mails.tsinghua.edu.cn, hexiao@tsinghua.edu.cn).

Zidong Wang is with the Department of Computer Science, Brunel University London, UB8 3PH Uxbridge, U.K. (e-mail: zidong.wang@brunel.ac.uk).

Zhen Shen is with State Key Laboratory of Multimodal Artificial Intelligence Systems, Beijing Engineering Research Center of Intelligent Systems and Technology, Institute of Automation, Chinese Academy of Sciences (e-mail: zhen.shen@ia.ac.cn).

NOMENCLATURE

x	System state vector
u	Control input vector
$f(x)$	System drift vector field
$g(x)$	Control input vector field
U	Admissible control input set
\mathcal{R}	Unsafe region in state space
$B(x)$	Control barrier function (CBF)
r	Relative degree of the CBF
$\alpha(\cdot)$	Class \mathcal{K} function
$L_f^r B$	r -th order Lie derivative of B along f
ψ_i	Recursive functions for HOCBF
C_i	The i -th associated safe set for HOCBF
$\nabla_x^r B$	r -th order gradient of B w.r.t. x
u_r	Reference control input
u_{safe}	Safety-filtered control input
$\ \cdot\ _2$	Euclidean norm or spectral norm
N_1	Number of node groups in RVFL network
N_2	Number of nodes per group in RVFL network
\tilde{x}	Extended feature vector
\tilde{y}	One-hot safety label vector
W_e	Enhancement layer weights of RVFL
b_e	Enhancement layer biases of RVFL
$\phi(\cdot)$	Activation function
A	Extended data matrix
Y	Ground-truth label matrix
$\hat{Y}(x)$	Prediction for the state x
W_b	Output weight matrix of RVFL
λ	Regularization parameter
c_1	Penalty cost for false negatives (misclassifying unsafe)
c_2	Penalty cost for false positives (misclassifying safe)
C	Misclassification cost matrix
$\text{tr}(\cdot)$	Matrix trace operator
L	Lipschitz constant
$\mathcal{B}(x_i, \delta_i)$	Neighborhood with radius δ_i centered at x_i
t	Continuous time index
τ	Discrete time index

I. INTRODUCTION

THE safety of dynamic systems has long been a central topic in autonomous systems research and is commonly defined as the capability of a system to prevent harm to personnel, equipment, or the environment [1], [2]. With continued advances in modern intelligent control theory, operational safety has become a key factor in the successful execution

of tasks by intelligent agents (e.g., robots) [3]–[7]. In safety-critical applications, it is typically essential to first assess the safety of system states effectively, followed by the design of control algorithms aimed at mitigating potential risks [8]. As a result, the synthesis of control algorithms that explicitly ensure safety-critical operation has emerged as a crucial research direction.

The safety of control systems can be represented by the constraints in states and is often specified through invariant sets [9], [10]. Within this framework, control barrier functions (CBFs) have recently become as a promising approach for safety enforcement, owing to their formal theoretical guarantees and real-time implementability [11]–[13]. By explicitly incorporating control inputs, CBFs extend classical barrier functions and enable the satisfaction of safety conditions through suitable control modifications [14], [15]. Given a predefined safety set and a nominal controller that does not explicitly address safety, CBF-based methods typically formulate a quadratic programming (QP) problem [16]. In this formulation, the CBF condition is imposed as a constraint while deviations from the nominal controller are minimized. Building on this paradigm, CBFs have been successfully applied to robotic manipulation [17], autonomous driving [18], unmanned aerial vehicle control [19], and satellite trajectory optimization [20], demonstrating strong empirical performance.

A key prerequisite for CBF-based methods is the availability of accurate knowledge of unsafe regions in the system state space and their explicit mathematical representation [20]–[24]. Once such regions are characterized, control inputs can be directly synthesized from the corresponding safe sets. However, owing to the complexity of real-world systems and the inherent randomness and non-stationarity of their operating environments, unsafe regions are often irregular and time-varying [25]–[27]. These properties render the derivation of closed-form analytical descriptions particularly challenging. Even when analytical expressions are attainable, they may involve non-smooth functions (e.g., piecewise definitions), which violate the differentiability requirements of standard CBFs. Furthermore, in many practical scenarios, explicit functional constraints are unavailable; instead, the system relies on discrete raw data, such as obstacle information from LiDAR scans or 3D point clouds from depth cameras. Consequently, a growing body of recent work has emphasized learning unsafe regions and constructing corresponding CBFs as important research problems [28]–[30].

To learn unsafe regions, recent studies have explored data-driven approaches based on sampling and machine learning techniques. In these studies, datasets consisting of system states and safety levels are collected through sensor measurements or human-in-the-loop feedback. A classifier is then trained to construct the corresponding CBFs. Under the paradigm, several methods based on support vector machines (SVMs) and multilayer perceptrons (MLPs) have been developed for CBF synthesis [31]–[35]. Despite these advances, several limitations remain. In many practical scenarios, safety constraints and human understanding of potential hazards evolve over time [2], [36], thereby imposing stringent requirements on the rapid adaptability of learning methods.

However, most existing approaches rely on batch training and lack the capability for incremental updates. Moreover, explicit gradient expressions are typically unavailable, which limits their applicability in subsequent analysis and control synthesis, such as the evaluation of Lipschitz properties and other safety-related characteristics.

To address the aforementioned limitations, we propose SafeLink, a novel real-time safety-critical control framework that constructs adaptive CBFs to handle dynamically changing safety threats. SafeLink is built on the random vector functional link (RVFL) network, a shallow, wide neural network with an explicit analytical form and universal approximation capability [37]–[39]. The main contributions of this work are as follows:

- 1) A cost-sensitive incremental RVFL network is employed to construct the CBF using a dataset comprising both safe and unsafe states. A novel objective function is introduced to incorporate cost sensitivity, ensuring comprehensive representation of unsafe regions.
- 2) Under static unsafe region scenarios, the Lipschitz continuity of the constructed CBF and the resulting control input is rigorously established. Moreover, theoretical guarantees are provided demonstrating that the proposed CBF is capable of correctly classifying all unsafe samples and accurately representing the unsafe regions.
- 3) Incremental update theorems are established for scenarios in which unsafe regions dynamically expand or contract, enabling real-time adaptation of the CBF to time-varying safety constraints.

The remainder of this paper is organized as follows. Section II introduces the preliminaries on CBFs and RVFL networks. Section III presents the proposed safety-critical control framework. Section IV reports experimental results obtained on a two-link manipulator system. Finally, Section V concludes the paper.

II. PRELIMINARIES

A. Control Barrier Functions

Consider the following affine control system:

$$\dot{\mathbf{x}} = \mathbf{f}(\mathbf{x}) + \mathbf{g}(\mathbf{x})\mathbf{u}, \quad (1)$$

where $\mathbf{x} \in \mathbb{R}^n$ denotes the system state, $\mathbf{f} : \mathbb{R}^n \rightarrow \mathbb{R}^n$ and $\mathbf{g} : \mathbb{R}^n \rightarrow \mathbb{R}^{n \times q}$ are locally Lipschitz continuous vector fields, and $\mathbf{u} \in U \subseteq \mathbb{R}^q$ denotes the control input. The admissible control input set is defined as

$$U := \{\mathbf{u} \in \mathbb{R}^q : \mathbf{u}_{\min} \leq \mathbf{u} \leq \mathbf{u}_{\max}\}, \quad (2)$$

where $\mathbf{u}_{\min}, \mathbf{u}_{\max} \in \mathbb{R}^q$, and the inequalities are interpreted element-wise.

Definition 1. (*Unsafe region*) A set $\mathcal{R} \subset \mathbb{R}^n$ is defined as an unsafe region if it contains all states that violate the safety requirements or physical constraints of the system. A state \mathbf{x} is referred to as unsafe if $\mathbf{x} \in \mathcal{R}$.

Definition 2. (*Relative Degree*) The relative degree of a differentiable function $B : \mathbb{R}^n \rightarrow \mathbb{R}$ with respect to system (1)

is the number of times it needs to be differentiated along the system dynamics until the control \mathbf{u} explicitly appears.

Definition 3. A safe set $C = \mathcal{R}^c \subset \mathbb{R}^n$ is said to be forward invariant for system (1) if all solutions starting at any $\mathbf{x}(t_0) \in C$ satisfy $\mathbf{x}(t) \in C, \forall t \geq t_0$.

Let

$$C := \{\mathbf{x} \in \mathbb{R}^n : B(\mathbf{x}) \geq 0\}, \quad (3)$$

where $B : \mathbb{R}^n \rightarrow \mathbb{R}$ is a continuously differentiable function.

Definition 4. (Control barrier function [12]) Given the safe set C defined in Eq. (3), a function $B(\mathbf{x})$ is called a control barrier function (CBF) for system (1) if there exists a class \mathcal{K} function α such that

$$\sup_{\mathbf{u} \in U} [L_f B(\mathbf{x}) + L_g B(\mathbf{x})\mathbf{u} + \alpha(B(\mathbf{x}))] \geq 0, \quad \forall \mathbf{x} \in C. \quad (4)$$

Lemma 1. [40] Given a CBF $B(\mathbf{x})$ as defined in Def. 4, with the associated safe set C specified by Eq. (3), if $\mathbf{x}(t_0) \in C$, then any Lipschitz continuous control input $\mathbf{u}(t)$ satisfying the constraint in (4) for all $t \geq t_0$ renders the set C forward invariant for system (1).

B. High-order Control Barrier Functions

Consider a control barrier function $B(\mathbf{x})$ with relative degree r . Define $\psi_0(\mathbf{x}) := B(\mathbf{x})$, and introduce a sequence of functions $\psi_i : \mathbb{R}^n \rightarrow \mathbb{R}, i \in \{1, \dots, r-1\}$. The time derivative of each function is given by $\dot{\psi}_{i-1}(\mathbf{x}) = \frac{\partial \psi_{i-1}}{\partial \mathbf{x}} \dot{\mathbf{x}}$, which leads to the recursive definition:

$$\psi_i(\mathbf{x}) := \dot{\psi}_{i-1}(\mathbf{x}) + \alpha_i(\psi_{i-1}(\mathbf{x})), i \in \{1, \dots, r-1\}, \quad (5)$$

where each $\alpha_i(\cdot)$ is a class \mathcal{K} function.

Associated with Eq. (5), define a sequence of sets $C_i, i \in \{1, \dots, r\}$, as:

$$C_i := \{\mathbf{x} \in \mathbb{R}^n : \psi_{i-1}(\mathbf{x}) \geq 0\}, i \in \{1, \dots, r\}. \quad (6)$$

Definition 5. (High Order Control Barrier Function [41]) Let the sets C_1, C_2, \dots, C_r be defined by Eq. (6), and let the functions $\psi_1(\mathbf{x}), \dots, \psi_{r-1}(\mathbf{x})$ be defined by Eq. (5). A function $B : \mathbb{R}^n \rightarrow \mathbb{R}$ is called a high order control barrier function (HOCBF) of relative degree r for system (1) if there exist differentiable class \mathcal{K} functions $\alpha_i, i \in \{1, \dots, r-1\}$, and a class \mathcal{K} function α_r such that

$$\sup_{\mathbf{u} \in U} [L_f^r B(\mathbf{x}) + L_g L_f^{r-1} B(\mathbf{x})\mathbf{u} + \mathcal{O}(B(\mathbf{x})) + \alpha_r(\psi_{r-1}(\mathbf{x}))] \geq 0, \quad \forall \mathbf{x} \in C_1 \cap C_2 \cap \dots \cap C_r, \quad (7)$$

where $\mathcal{O}(B(\mathbf{x})) = \sum_{i=1}^{r-1} L_f^i (\alpha_{r-i} \circ \psi_{r-i-1})(\mathbf{x})$, and $B(\mathbf{x})$ satisfies $L_g L_f^{r-1} B(\mathbf{x}) \neq 0$ on the boundary of the set $C_1 \cap C_2 \cap \dots \cap C_r$.

Lemma 2. [41] Given a HOCBF $B(\mathbf{x})$ as defined in Def. 5, with the associated sets C_1, C_2, \dots, C_r defined by Eq. (6), if $\mathbf{x}(t_0) \in C_1 \cap C_2 \cap \dots \cap C_r$, then any Lipschitz continuous control input $\mathbf{u}(t) \in \mathcal{U}$ satisfying

$$L_f^r B(\mathbf{x}) + L_g L_f^{r-1} B(\mathbf{x})\mathbf{u}(t) + \mathcal{O}(B(\mathbf{x})) + \alpha_r(\psi_{r-1}(\mathbf{x})) \geq 0 \quad (8)$$

for all $t \geq t_0$ renders the set $C_1 \cap C_2 \cap \dots \cap C_r$ forward invariant for system (1).

Let \mathbf{u}_r denote a reference control input, which may be obtained from optimal control or control Lyapunov function-based methods. The primary objective of \mathbf{u}_r is to drive the system toward a desired state or to accomplish a specific task, such as trajectory tracking or stabilization. However, since \mathbf{u}_r is typically designed without explicit consideration of safety constraints, its direct application may result in safety violations. To ensure safety, the control input is computed by solving the following quadratic program:

$$\begin{aligned} \mathbf{u}_{safe} = \operatorname{argmin}_{\mathbf{u} \in U} & \|\mathbf{u} - \mathbf{u}_r\|_2^2 \\ \text{s.t.} & \begin{cases} L_f B(\mathbf{x}) + L_g B(\mathbf{x})\mathbf{u} + \alpha(B(\mathbf{x})) \geq 0, \text{ if } r = 1, \\ L_f^r B(\mathbf{x}) + L_g L_f^{r-1} B(\mathbf{x})\mathbf{u} + \mathcal{O}(B(\mathbf{x})) \\ + \alpha_r(\psi_{r-1}(\mathbf{x})) \geq 0, \text{ if } r > 1. \end{cases} \end{aligned} \quad (9)$$

C. Random Vector Functional Link Network

The random vector functional link (RVFL) network is a shallow neural network architecture composed of an input layer, a hidden enhancement layer, and an output layer [37]. The enhancement layer consists of N_1 node groups, each containing N_2 nodes, resulting in a total of $M = N_1 N_2$ enhancement features. RVFL training is performed through ridge regression, which admits a closed-form solution [42].

Suppose a dataset of state samples $\{\mathbf{x}_i\}_{i=1}^N$ is given together with corresponding safety labels, where each $\mathbf{x}_i \in \mathbb{R}^n$ denotes an n -dimensional system state. Let $\tilde{\mathbf{x}} \in \mathbb{R}^{(n+N_1 N_2) \times 1}$ denote the extended feature vector formed by concatenating the original state \mathbf{x} and its enhancement features \mathbf{Z} , and let $\tilde{\mathbf{y}}$ represent the one-hot coding of the safety label:

$$\tilde{\mathbf{x}} = \begin{bmatrix} \mathbf{x}^\top \\ \mathbf{Z}^\top \end{bmatrix} = \begin{bmatrix} \mathbf{x}^\top \\ \phi(\mathbf{x}^\top \mathbf{W}_{e_1} + \mathbf{b}_{e_1}) \\ \phi(\mathbf{x}^\top \mathbf{W}_{e_2} + \mathbf{b}_{e_2}) \\ \vdots \\ \phi(\mathbf{x}^\top \mathbf{W}_{e_{N_1}} + \mathbf{b}_{e_{N_1}}) \end{bmatrix}, \quad (10)$$

$$\tilde{\mathbf{y}} = \begin{cases} [1, 0], & \text{if } \mathbf{x} \text{ is in unsafe regions,} \\ [0, 1], & \text{if } \mathbf{x} \text{ is in safe regions,} \end{cases}$$

where $\phi(\cdot) : \mathbb{R} \rightarrow \mathbb{R}$ denotes the activation function. The matrices $\mathbf{W}_e = [\mathbf{W}_{e_1}, \mathbf{W}_{e_2}, \dots, \mathbf{W}_{e_{N_1}}]$ and $\mathbf{b}_e = [\mathbf{b}_{e_1}, \mathbf{b}_{e_2}, \dots, \mathbf{b}_{e_{N_1}}]$ represent the randomly initialized and fixed weights and biases of the enhancement layer. For each group $i \in \{1, \dots, N_1\}$, the weight matrix $\mathbf{W}_{e_i} \in \mathbb{R}^{n \times N_2}$ and bias vector $\mathbf{b}_{e_i} \in \mathbb{R}^{1 \times N_2}$ define the corresponding N_2 enhancement nodes. If the input to $\phi(\cdot)$ is a matrix, the activation function $\phi(\cdot)$ is applied element-wise.

Define the extended data matrix $\mathbf{A} \in \mathbb{R}^{N \times (n+N_1 N_2)}$ and the label matrix $\mathbf{Y} \in \mathbb{R}^{N \times 2}$ as

$$\mathbf{A} = [\tilde{\mathbf{x}}_1, \tilde{\mathbf{x}}_2, \dots, \tilde{\mathbf{x}}_N]^\top, \quad \mathbf{Y} = [\tilde{\mathbf{y}}_1, \tilde{\mathbf{y}}_2, \dots, \tilde{\mathbf{y}}_N]^\top, \quad (11)$$

where $\tilde{\mathbf{x}}_i \in \mathbb{R}^{(n+N_1N_2) \times 1}$ and $\tilde{\mathbf{y}}_i \in \mathbb{R}^{2 \times 1}$. The output weight matrix $\mathbf{W}_b \in \mathbb{R}^{(n+N_1N_2) \times 2}$ is obtained by solving the regularized least-squares problem

$$\mathbf{W}_b = \arg \min_{\mathbf{W}} \lambda \|\mathbf{W}\|_2^2 + \|\mathbf{A}\mathbf{W} - \mathbf{Y}\|_2^2, \quad (12)$$

which admits the closed-form solution

$$\mathbf{W}_b = (\lambda \mathbf{I} + \mathbf{A}^\top \mathbf{A})^{-1} \mathbf{A}^\top \mathbf{Y}. \quad (13)$$

For a given state point \mathbf{x} , the prediction vector is computed as $\hat{\mathbf{y}} = \tilde{\mathbf{x}}\mathbf{W}_b$. The state is classified as unsafe if the first component of $\hat{\mathbf{y}}$ exceeds the second; otherwise, it is classified as safe.

III. THE PROPOSED FRAMEWORK

This section presents the design of the proposed SafeLink framework, including the formulation of the objective function, the construction of the control barrier function, and its application to safety-critical control. Subsequently, several safety-related and update-related theorems underlying SafeLink are derived. An overview of the framework is illustrated in Fig. 1.

A. SafeLink Design for Static Unsafe Regions

To better accommodate safety-critical control requirements, a cost-sensitive incremental RVFL network is proposed by reformulating the objective function in Eq. (12).

Let c_1 denote the penalty parameter for misclassifying an unsafe state as safe (false negative), and let c_2 denote the penalty parameter for misclassifying a safe state as unsafe (false positive). The cost matrix is defined as:

$$\mathbf{C} = \begin{bmatrix} 0 & c_1 \\ c_2 & 0 \end{bmatrix}. \quad (14)$$

To explicitly emphasize the correct identification of unsafe samples, a novel cost-sensitive regularization term is introduced:

$$\mathcal{L}_{\text{unsafe}} \triangleq \text{tr}(\mathbf{A}\mathbf{W}\mathbf{C}^\top \mathbf{Y}^\top), \quad (15)$$

where $\text{tr}(\cdot)$ denotes the matrix trace operator. In safety-critical settings, it is typically desirable to set $c_1 \gg c_2$, thereby imposing a substantially higher penalty on hazardous false-negative classifications.

This formulation is motivated by projection and correlation analysis. Intuitively, the proposed term measures the alignment between the predicted outputs and the ground-truth labels through the cost matrix. To illustrate, consider an unsafe sample with one-hot label $\tilde{\mathbf{y}} = [1, 0]^\top$. Given a cost matrix where $c_2 = 0$, if the model correctly predicts $\hat{\mathbf{y}} = [1, 0]^\top$, the term $\text{tr}(\tilde{\mathbf{y}}\mathbf{C}^\top \hat{\mathbf{y}}^\top)$ vanishes, yielding no penalty. Conversely, if the model erroneously predicts $\hat{\mathbf{y}} = [0, 1]^\top$ (misclassifying *unsafe* as *safe*), the penalty scales to c_1 .

When generalized to the entire dataset, the diagonal elements of $\mathbf{A}\mathbf{W}\mathbf{C}^\top \mathbf{Y}^\top$ represent the individual cost-weighted mismatches for each sample. Under the assumption of independent and identically distributed (i.i.d.) samples, the off-diagonal elements represent cross-sample correlations that remain uninformative for optimizing the classification accuracy

of unsafe samples. Consequently, the trace operator serves to aggregate these relevant prediction mismatches into a single scalar objective. The resulting cost-sensitive learning problem is formulated as

$$\mathbf{W}_b = \arg \min_{\mathbf{W}} \lambda \|\mathbf{W}\|_2^2 + \|\mathbf{A}\mathbf{W} - \mathbf{Y}\|_2^2 + 2 \text{tr}(\mathbf{A}\mathbf{W}\mathbf{C}^\top \mathbf{Y}^\top). \quad (16)$$

It is worth noting that expressing the cost-sensitive term in this trace-based form, rather than as a summation of discrete sample-level penalties, serves a critical purpose. Conventional cost-sensitive SVMs or MLPs often rely on indicator-based loss terms such as $\sum I(y_i \neq \hat{y}_i)$, which are non-differentiable with respect to the weight matrix \mathbf{W} . Such formulations do not yield closed-form solutions and are unsuitable for incremental updates. In contrast, the proposed term $\text{tr}(\mathbf{A}\mathbf{W}\mathbf{C}^\top \mathbf{Y}^\top)$ is continuous and differentiable with respect to \mathbf{W} , which is essential for deriving analytical solutions and enabling real-time incremental learning.

Based on convex optimization theory, the optimal weight matrix \mathbf{W}_b in Eq. (16) can be derived as follows:

$$\mathbf{W}_b = \underbrace{(\lambda \mathbf{I} + \mathbf{A}^\top \mathbf{A})^{-1}}_{\mathbf{K}} \underbrace{(\mathbf{A}^\top \mathbf{Y} - \mathbf{A}^\top \mathbf{Y}\mathbf{C})}_{\mathbf{Q}}, \quad (17)$$

where the two terms are denoted by \mathbf{K} and \mathbf{Q} , respectively, for notational convenience.

For a state point \mathbf{x} , referring to Eqs. (10), (11) and (17), the prediction confidence $\hat{\mathbf{Y}}(\mathbf{x}) \in \mathbb{R}^{1 \times 2}$ is computed as

$$\begin{aligned} \hat{\mathbf{Y}}(\mathbf{x}) &= \tilde{\mathbf{x}}^\top \mathbf{W}_b \\ &= \tilde{\mathbf{x}}^\top (\lambda \mathbf{I} + \mathbf{A}^\top \mathbf{A})^{-1} (\mathbf{A}^\top \mathbf{Y} - \mathbf{A}^\top \mathbf{Y}\mathbf{C}) \\ &= \mathbf{x}^\top \mathbf{W}_{b_0} + \sum_{i=1}^{N_1} \sum_{j=1}^{N_2} \phi(\mathbf{x}^\top \mathbf{W}_{e_{i,j}} + b_{e_{i,j}}) \mathbf{W}_{b_{i,j}}, \end{aligned} \quad (18)$$

where $\mathbf{W}_{b_0} \in \mathbb{R}^{n \times 2}$ is the submatrix of \mathbf{W}_b corresponding to input \mathbf{x}^\top ; $\mathbf{W}_{b_{i,j}} \in \mathbb{R}^{1 \times 2}$ corresponds to the j -th feature node of the i -th feature group, similarly for $b_{e_{i,j}} \in \mathbb{R}$ and $\mathbf{W}_{e_{i,j}} \in \mathbb{R}^m$.

The vector $\hat{\mathbf{Y}}(\mathbf{x})$ quantifies the degree of unsafety: unsafe states yield predictions close to $[1, 0]^\top$, whereas safe states yield predictions close to $[0, 1]^\top$. Since $\hat{\mathbf{Y}}(\mathbf{x})$ is a vector and the CBF must be a scalar, the prediction must be mapped to a scalar value. This mapping is designed such that $B(\mathbf{x}) < 0$ when the first component of $\hat{\mathbf{Y}}(\mathbf{x})$ exceeds the second, and $B(\mathbf{x}) > 0$ otherwise. For simplicity and to ensure $B(\mathbf{x})$ is continuous and differentiable with respect to \mathbf{x} , the CBF is constructed using the second component of the prediction vector:

$$B(\mathbf{x}) = 2\hat{\mathbf{Y}}(\mathbf{x}) [0 \ 1]^\top - 1. \quad (19)$$

To compute the safety-critical control input in (9), explicit gradients of the CBF are required. The first- and second-order derivatives of (19) are given by

$$\begin{aligned} \nabla_{\mathbf{x}} B &= 2\mathbf{W}_{b_0} [0, 1]^\top + \\ & 2 \sum_{i=1}^{N_1} \sum_{j=1}^{N_2} \mathbf{W}_{b_{i,j}} \begin{bmatrix} 0 \\ 1 \end{bmatrix} \phi'(\mathbf{x}^\top \mathbf{W}_{e_{i,j}} + b_{e_{i,j}}) \mathbf{W}_{e_{i,j}}, \end{aligned}$$

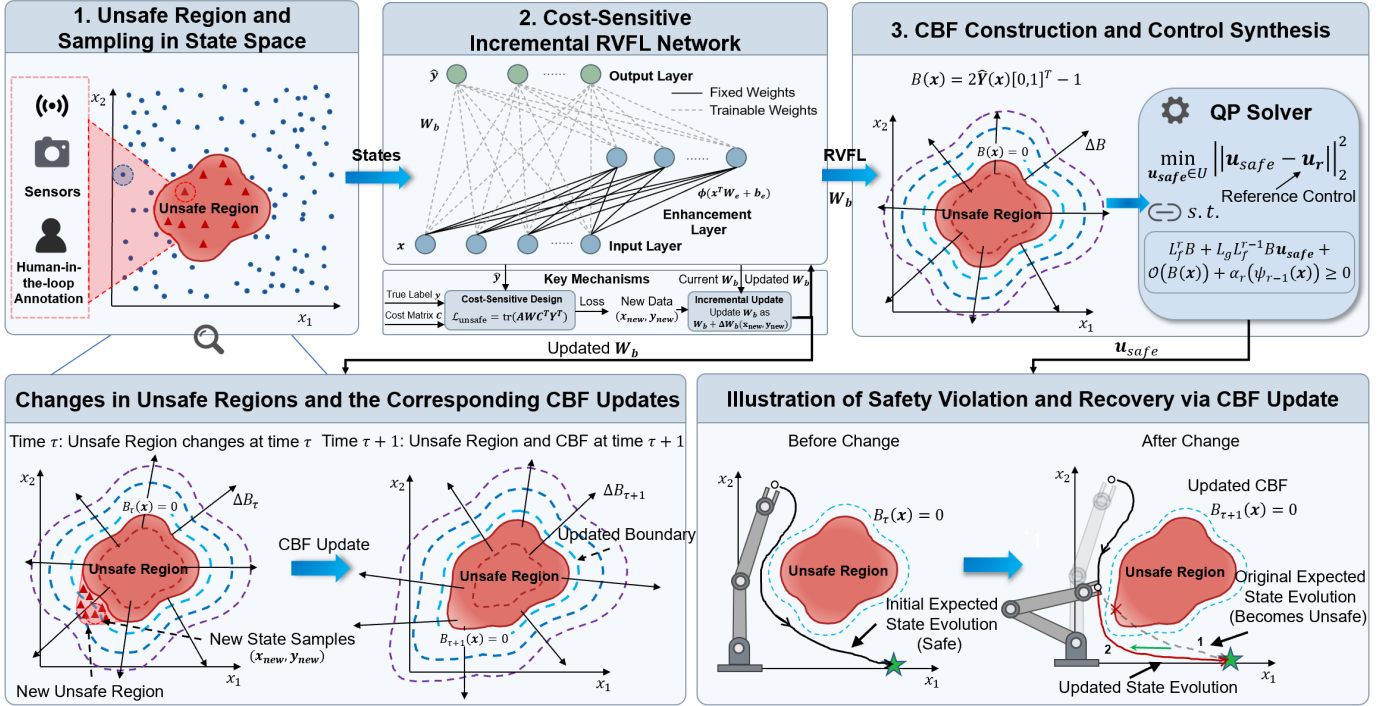


Fig. 1: Diagram of SafeLink. SafeLink first collects safe and unsafe state samples in the state space. Then, a cost-sensitive and incremental RVFL network is designed to train on these samples for CBF construction, where a QP solver is employed to output safe control inputs. When the unsafe region changes, the constructed CBF can be rapidly updated using samples from the new unsafe region to ensure system safety.

$$\begin{aligned} \nabla_{\mathbf{x}}^2 B &= \frac{\partial^2 B}{\partial \mathbf{x} \partial \mathbf{x}^\top} \\ &= 2 \sum_{i=1}^{N_1} \sum_{j=1}^{N_2} \mathbf{W}_{b_{i,j}} \begin{bmatrix} 0 \\ 1 \end{bmatrix} \phi''(\mathbf{x}^\top \mathbf{W}_{e_{i,j}} + b_{e_{i,j}}) \mathbf{W}_{e_{i,j}} \mathbf{W}_{e_{i,j}}^\top. \end{aligned} \quad (20)$$

If the CBF has relative degree 1 with respect to the system, the Lie derivatives $L_f B = \nabla_{\mathbf{x}} B^\top \cdot \mathbf{f}(\mathbf{x})$ and $L_g B = \nabla_{\mathbf{x}} B^\top g(\mathbf{x})$ are directly substituted into Eq. (9) to solve for \mathbf{u}_{safe} . For systems with relative degree 2, the required derivatives are

$$L_f^2 B = \nabla_{\mathbf{x}}(L_f B) \cdot \mathbf{f}, \quad L_g L_f B = \nabla_{\mathbf{x}}(L_f B) \cdot \mathbf{g}. \quad (21)$$

with

$$\nabla_{\mathbf{x}}(L_f B) = \nabla_{\mathbf{x}}^2 B^\top \cdot \mathbf{f} + \left(\frac{\partial \mathbf{f}}{\partial \mathbf{x}^\top} \right)^\top \cdot \nabla_{\mathbf{x}} B. \quad (22)$$

For higher relative degrees, Lie derivatives can be computed analogously. It is noted that for a system with a relative order r , the activation function must be selected to be r -times differentiable. The safety-critical control input \mathbf{u}_{safe} is finally obtained by solving the QP in (9), as illustrated in Fig. 1. The Lipschitz continuity of \mathbf{u}_{safe} under mild conditions is established in Theorem 1.

Theorem 1. Assume that the activation function $\phi(\cdot)$ is r -times differentiable and its derivatives up to order r are Lipschitz continuous. Then, the learned CBF $B(\mathbf{x})$ and its derivatives $\nabla_{\mathbf{x}}^p B(\mathbf{x})$ for $p \in \{1, \dots, r\}$ are Lipschitz continuous. Furthermore, if the Jacobian matrix $J_f(\mathbf{x})$ and the class- \mathcal{K} functions $\alpha_i(\cdot)$ are Lipschitz continuous, and the set $C := \{\mathbf{x} \in \mathbb{R}^n \mid B(\mathbf{x}) \geq 0\}$ is compact, then the safety-critical

control input \mathbf{u}_{safe} defined in Eq. (9) is Lipschitz continuous, provided that \mathbf{u}_r is Lipschitz continuous and that feasible solutions for Eq. (9) exist (i.e., there exists $\mathbf{u} \in \mathcal{U}$ such that the constraint is satisfied).

Proof Flatten the $N_1 \times N_2$ enhancement nodes into $M = N_1 N_2$, so that Eq. (18) becomes

$$\hat{Y}(\mathbf{x}) = \mathbf{x}^\top \mathbf{W}_{b_0} + \sum_{k=1}^M \phi(\mathbf{x}^\top \mathbf{W}_{e,k} + b_{e,k}) \mathbf{W}_{b,k}, \quad (23)$$

where the index k is defined as $k = (i-1)N_2 + j$.

Suppose $\phi(\cdot)$ is Lipschitz continuous with constant L_ϕ , it follows that for any $\mathbf{x}_1, \mathbf{x}_2$,

$$\begin{aligned} \|\hat{Y}(\mathbf{x}_1) - \hat{Y}(\mathbf{x}_2)\|_2 &\leq \|(\mathbf{x}_1^\top - \mathbf{x}_2^\top) \mathbf{W}_{b,0}\|_2 \\ &+ \sum_{k=1}^M \|(\phi(\mathbf{x}_1^\top \mathbf{W}_{e,k} + b_{e,k}) - \phi(\mathbf{x}_2^\top \mathbf{W}_{e,k} + b_{e,k})) \mathbf{W}_{b,k}\|_2 \\ &\leq (\|\mathbf{W}_{b,0}\|_2 + \sum_{k=1}^M L_\phi \|\mathbf{W}_{e,k}\|_2 \cdot \|\mathbf{W}_{b,k}\|_2) \cdot \|\mathbf{x}_1 - \mathbf{x}_2\|_2. \end{aligned} \quad (24)$$

with Lipschitz constant

$$L_{\hat{Y}} = \|\mathbf{W}_{b,0}\|_2 + \sum_{k=1}^M L_\phi \|\mathbf{W}_{e,k}\|_2 \|\mathbf{W}_{b,k}\|_2. \quad (25)$$

Since B is a linear combination of \hat{Y} , it is Lipschitz with constant $L_B = 2L_{\hat{Y}}$. Similarly, for p -th order derivatives,

$\nabla_{\mathbf{x}}^p B$ is Lipschitz with

$$L_{\nabla_{\mathbf{x}}^p B} = 2 \sum_{k=1}^M L_{\phi^{(p)}} \|\mathbf{W}_{b,k}\|_2 \cdot \|\mathbf{W}_{e,k}\|_2^{p+1}, \quad (26)$$

where $\phi^{(p)}$ denotes the p -th derivative of $\phi(\cdot)$.

By the *Karush–Kuhn–Tucker (KKT)* condition, the solution to Eq. (9) can be expressed as

$$\mathbf{u}_{safe}(\mathbf{x}) = \begin{cases} \mathbf{u}_r, & d(\mathbf{x}) \geq 0, \\ \mathbf{u}_r - \frac{d(\mathbf{x})}{\|b(\mathbf{x})\|_2^2} b(\mathbf{x}), & d(\mathbf{x}) < 0, \end{cases} \quad (27)$$

where

$$\begin{aligned} d(\mathbf{x}) &= L_g L_f^{r-1} B \cdot \mathbf{u}_r + L_f^r B + \mathcal{O}(B) + \alpha_r (\psi_{r-1}) \\ b(\mathbf{x}) &= L_g L_f^{r-1} B. \end{aligned}$$

Since \mathbf{u}_r is Lipschitz continuous, $\mathbf{u}_{safe}(\mathbf{x})$ is Lipschitz continuous whenever $d(\mathbf{x}) \geq 0$. Moreover, since $\alpha(\cdot)$, \mathbf{f} , \mathbf{g} , and $J_f(\mathbf{x})$ are Lipschitz continuous, and C is compact, it follows that $d(\mathbf{x})$ and $b(\mathbf{x})$ are Lipschitz continuous. In particular, compactness of C guarantees the existence of a constant $M_d > 0$ such that $|d(\mathbf{x})| \leq M_d$. Furthermore, the condition $L_g L_f^{r-1} B \neq 0$ implies the existence of a constant $m_b > 0$ such that $\|L_g L_f^{r-1} B\|_2 > m_b$ over C . If L_d and L_b denote the Lipschitz constants of $d(\mathbf{x})$ and $b(\mathbf{x})$, respectively. Then the Lipschitz constant of $\mathbf{u}_r - \frac{d(\mathbf{x})}{\|b(\mathbf{x})\|_2^2} b(\mathbf{x})$ is $L_{u_r} + L_d/m_b + M_d L_b/m_b^2$. Finally, since $\lim_{d(\mathbf{x}) \rightarrow 0^-} \mathbf{u}_{safe}(\mathbf{x}) = \mathbf{u}_r = \lim_{d(\mathbf{x}) \rightarrow 0^+} \mathbf{u}_{safe}(\mathbf{x})$, $\mathbf{u}_{safe}(\mathbf{x})$ is continuous at $d(\mathbf{x}) = 0$. Therefore, $\mathbf{u}_{safe}(\mathbf{x})$ is Lipschitz continuous. ■

To further analyze the safety properties of the learned CBF, the effect of the misclassification cost c_1 on the training set \mathcal{X} is investigated. Let $\mathbf{H} \in \mathbb{R}^{N \times N}$ denote the hat matrix associated with the regularized least-squares problem, defined as

$$\mathbf{H} = \mathbf{A}(\lambda \mathbf{I} + \mathbf{A}^\top \mathbf{A})^{-1} \mathbf{A}^\top, \quad (28)$$

where h_{ki} denotes the (k, i) -th element of \mathbf{H} , representing the influence of the i -th training sample on the prediction corresponding to the k -th sample. As known, for $\lambda > 0$, all eigenvalues of \mathbf{H} lie in the interval $[0, 1)$, which implies $0 \leq h_{kk} < 1$. To guarantee that the learned CBF correctly classifies all unsafe training samples as $c_1 \rightarrow \infty$, the following mild assumption on the feature-space representation is introduced.

Assumption 1. For any unsafe training sample $\mathbf{x}_k \in \mathcal{X}_u$, the aggregate influence from the unsafe set \mathcal{X}_u is strictly positive. That is, there exists a constant $\epsilon > 0$ such that $S_k = \sum_{i \in \mathcal{X}_u} h_{ki} \geq \epsilon$.

Remark 1. This assumption implies that the self-influence h_{kk} , together with positive correlations contributed by neighboring unsafe samples in the feature space, dominates any potential negative correlations. Such behavior is a standard property in stable feature mapping layers and is commonly satisfied in practice.

Theorem 2. Under Assumption 1, let $B(\mathbf{x})$ be the learned CBF. As the misclassification cost for unsafe samples $c_1 \rightarrow \infty$, the learned CBF satisfies $B(\mathbf{x}_k) < 0$ for all unsafe training samples $\mathbf{x}_k \in \mathcal{X}_u$.

Proof Define $\mathbf{R} = \mathbf{Y} - \mathbf{Y}\mathbf{C} \in \mathbb{R}^{N \times 2}$. Given the one-hot label $\tilde{\mathbf{y}}_i$ in Eq. (9) and the cost matrix \mathbf{C} in Eq. (13), the i -th row of \mathbf{R} , denoted as \mathbf{r}_i^\top , is determined as follows:

- For an unsafe sample $\mathbf{x}_i \in \mathcal{X}_u$ with label $\tilde{\mathbf{y}}_i = [1, 0]$:

$$\mathbf{r}_i^\top = [1, 0] - [1, 0] \begin{bmatrix} 0 & c_1 \\ c_2 & 0 \end{bmatrix} = [1, -c_1].$$

- For a safe sample $\mathbf{x}_j \in \mathcal{X}_s$ where $\tilde{\mathbf{y}}_j = [0, 1]$:

$$\mathbf{r}_j^\top = [0, 1] - [0, 1] \begin{bmatrix} 0 & c_1 \\ c_2 & 0 \end{bmatrix} = [-c_2, 1].$$

Since the CBF $B(\mathbf{x})$ in Eq. (17) is constructed from the second component of the prediction confidence $\hat{\mathbf{Y}}(\mathbf{x})$, only the second column of \mathbf{R} is relevant. Denote this column by $\mathbf{a}_2 \in \mathbb{R}^N$, whose entries satisfy

$$a_{2,i} = \begin{cases} -c_1, & \mathbf{x}_i \in \mathcal{X}_u, \\ 1, & \mathbf{x}_i \in \mathcal{X}_s, \end{cases} \quad (29)$$

where \mathcal{X}_s denotes the set of safe training samples.

According to Eq. (18), the second column of the prediction confidence for all training samples is given by $\hat{\mathbf{y}}_2 = \mathbf{H}\mathbf{a}_2$. For a particular unsafe sample $\mathbf{x}_k \in \mathcal{X}_u$, the prediction $\hat{Y}_2(\mathbf{x}_k)$ can be expanded as:

$$\hat{Y}_2(\mathbf{x}_k) = \sum_{i=1}^N h_{ki} a_{2,i} = \sum_{i \in \mathcal{X}_u} h_{ki} (-c_1) + \sum_{j \in \mathcal{X}_s} h_{kj} (1). \quad (30)$$

Rearranging terms yields

$$\hat{Y}_2(\mathbf{x}_k) = -c_1 S_k + \sum_{j \in \mathcal{X}_s} h_{kj}, \quad (31)$$

where $S_k := \sum_{i \in \mathcal{X}_u} h_{ki}$.

By Assumption 1, $S_k \geq \epsilon > 0$. Therefore, as $c_1 \rightarrow \infty$, the dominant term $-c_1 S_k$ tends to $-\infty$, while the remaining term remains bounded. Since the CBF $B(\mathbf{x}) = 2\hat{Y}_2(\mathbf{x}) - 1$, it follows that

$$\lim_{c_1 \rightarrow \infty} B(\mathbf{x}_k) = \lim_{c_1 \rightarrow \infty} 2 \left(-c_1 S_k + \sum_{j \in \mathcal{X}_s} h_{kj} \right) - 1 = -\infty.$$

Consequently, there exists a constant \bar{c}_1 such that $B(\mathbf{x}_k) < 0$ for all $c_1 > \bar{c}_1$ and all $\mathbf{x}_k \in \mathcal{X}_u$. ■

The following corollary exploits the Lipschitz continuity of the learned CBF. It extends the pointwise identification guarantee of unsafe samples in Theorem 2 to a neighborhood around each unsafe training sample.

Corollary 1. Let L_B denote the Lipschitz constant of the learned CBF $B(\mathbf{x})$. For any unsafe training sample $\mathbf{x}_i \in \mathcal{X}_u$, if $B(\mathbf{x}_i) < 0$ (otherwise, this condition can be enforced by increasing c_1), there exists a neighborhood $\mathcal{B}(\mathbf{x}_i, \delta_i)$ with radius

$$\delta_i = \frac{|B(\mathbf{x}_i)|}{L_B}$$

such that $B(\mathbf{x}) < 0$ for all $\mathbf{x} \in \mathcal{B}(\mathbf{x}_i, \delta_i)$.

Moreover, as $c_1 \rightarrow \infty$ and the number of state samples $N \rightarrow \infty$, the radius δ_i admits a positive lower bound for all $\mathbf{x}_i \in \mathcal{X}_u$. Consequently, increasing the sampling density of unsafe states guarantees that the union of these neighborhoods forms a continuous and conservative unsafe envelope over the unsafe region.

Proof By the Lipschitz continuity of $B(\mathbf{x})$ established in Theorem 1, for any $\mathbf{x} \in \mathbb{R}^n$ and any unsafe training sample $\mathbf{x}_i \in \mathcal{X}_u$, the following inequality holds:

$$B(\mathbf{x}) - B(\mathbf{x}_i) \leq |B(\mathbf{x}) - B(\mathbf{x}_i)| \leq L_B \|\mathbf{x} - \mathbf{x}_i\|_2. \quad (32)$$

It implies

$$B(\mathbf{x}) \leq B(\mathbf{x}_i) + L_B \|\mathbf{x} - \mathbf{x}_i\|_2. \quad (33)$$

Therefore, a sufficient condition for \mathbf{x} to be classified as unsafe, i.e., $B(\mathbf{x}) < 0$, is

$$B(\mathbf{x}_i) + L_B \|\mathbf{x} - \mathbf{x}_i\|_2 < 0. \quad (34)$$

Rearranging the inequality yields

$$\|\mathbf{x} - \mathbf{x}_i\|_2 < \frac{-B(\mathbf{x}_i)}{L_B} = \frac{|B(\mathbf{x}_i)|}{L_B} = \delta_i. \quad (35)$$

Hence, $B(\mathbf{x}) < 0$ holds for all $\mathbf{x} \in \mathcal{B}(\mathbf{x}_i, \delta_i)$.

Note that $B(\mathbf{x}_i) = 2\hat{Y}_2(\mathbf{x}_i) - 1$. Combined with Eq. 31, it implies that $|B(\mathbf{x}_i)| \rightarrow 2c_1 S_i$ as $c_1 \rightarrow \infty$.

To characterize the denominator L_B , the optimal weight matrix in (17) is rewritten by normalizing with the total sample size N :

$$\mathbf{W}_b = \left(\frac{\lambda}{N} \mathbf{I} + \frac{1}{N} \mathbf{A}^\top \mathbf{A} \right)^{-1} \frac{1}{N} \mathbf{A}^\top \mathbf{Y} (\mathbf{I} - \mathbf{C}). \quad (36)$$

As $c_1 \rightarrow \infty$, the spectral norm satisfies $\|\mathbf{I} - \mathbf{C}\|_2 \rightarrow c_1$. Meanwhile, by the law of large numbers, as $N \rightarrow \infty$, the data and label matrices satisfy the following convergence property:

$$\lim_{N \rightarrow \infty} \left(\frac{\lambda}{N} \mathbf{I} + \frac{1}{N} \mathbf{A}^\top \mathbf{A} \right)^{-1} \frac{1}{N} \mathbf{A}^\top \mathbf{Y} = \boldsymbol{\Sigma}_{xx}^{-1} \boldsymbol{\Sigma}_{xy},$$

where $\boldsymbol{\Sigma}_{xx} = \frac{1}{N} \mathbf{A}^\top \mathbf{A}$ and $\boldsymbol{\Sigma}_{xy} = \frac{1}{N} \mathbf{A}^\top \mathbf{Y}$ denote the feature covariance matrix and the feature–target cross-covariance matrix of the underlying data distribution, respectively. Thus, the Lipschitz constant satisfies $L_B \rightarrow 2c_1 C(\mathbf{W}_e, \mathbf{b}_e, \boldsymbol{\Sigma}_{xx}, \boldsymbol{\Sigma}_{xy})$, where $C(\mathbf{W}_e, \mathbf{b}_e, \boldsymbol{\Sigma}_{xx}, \boldsymbol{\Sigma}_{xy})$ is a constant determined by the enhancement layer and data distribution according to Eqs. (10), (18), (19) and (25).

As a result, the scaling factor c_1 cancels in the ratio defining δ_i , yielding

$$\lim_{c_1, N \rightarrow \infty} \delta_i = \frac{S_i}{C(\mathbf{W}_e, \mathbf{b}_e, \boldsymbol{\Sigma}_{xx}, \boldsymbol{\Sigma}_{xy})} \geq \frac{\epsilon}{C(\mathbf{W}_e, \mathbf{b}_e, \boldsymbol{\Sigma}_{xx}, \boldsymbol{\Sigma}_{xy})}, \quad (37)$$

which completes the proof. This result further indicates that sufficiently dense sampling of unsafe states yields full coverage of the unsafe region. ■

The above corollary shows that the learning procedure establishes a conservative approximation of the unsafe region in the state space. We now show that this approximation, when

combined with the CBF-based constraint, guarantees safety for the system.

Corollary 2. Suppose that by increasing the misclassification parameter c_1 and the sampling density as described in Corollary 1, the learned unsafe set $\hat{\mathcal{R}}_u := \{\mathbf{x} \in \mathbb{R}^n | B(\mathbf{x}) < 0\}$ satisfies the inclusion $\mathcal{R}_u \subseteq \hat{\mathcal{R}}_u$, where \mathcal{R}_u denotes the real unsafe region. Then, during any time interval over which \mathcal{R}_u and $B(\mathbf{x})$ remain unchanged, if the initial state satisfies $\mathbf{x}(t_0) \in \hat{\mathcal{C}}_s := \{\mathbf{x} \in \mathbb{R}^n | B(\mathbf{x}) \geq 0\} \cap \hat{\mathcal{C}}_2 \cap \dots \cap \hat{\mathcal{C}}_r$, where $\hat{\mathcal{C}}_2, \dots, \hat{\mathcal{C}}_r$ are defined as in Eqs. (5) and (6), it follows that $\mathbf{x}(t) \notin \mathcal{R}_u$ for all $t \geq t_0$.

Proof By assumption, the learned unsafe set is conservative, meaning $\mathcal{R}_u \subseteq \hat{\mathcal{R}}_u$. Consequently, the estimated safe set $\hat{\mathcal{C}}_s$ (the complement of $\hat{\mathcal{R}}_u$) is a subset of the real safe set \mathcal{C}_s (the complement of \mathcal{R}_u). By Nagumo’s Theorem, the control law in Eq. (9) ensures the forward invariance of $\hat{\mathcal{C}}_s \cap \hat{\mathcal{C}}_2 \cap \dots \cap \hat{\mathcal{C}}_r$ via the CBF condition. Therefore, starting from $\mathbf{x}(t_0) \in \hat{\mathcal{C}}_s \cap \hat{\mathcal{C}}_2 \cap \dots \cap \hat{\mathcal{C}}_r$, the state trajectory $\mathbf{x}(t)$ remains in $\hat{\mathcal{C}}_s$ for all future time. Since $\hat{\mathcal{C}}_s \subseteq \mathcal{C}_s$, it follows that $\mathbf{x}(t)$ also remains in \mathcal{C}_s for all $t \geq t_0$. Consequently, the system never enters the unsafe region \mathcal{R}_u , thereby guaranteeing safety. ■

B. SafeLink Update for Dynamic Unsafe Regions

We consider a discrete-time update setting indexed by $\tau \in \mathbb{Z}_{\geq 0}$, where each time step corresponds to the change of unsafe region. When the unsafe region evolves over time, SafeLink supports incremental updates using newly observed state samples and their associated safety labels, thereby avoiding retraining on the entire dataset. Such update mechanism is illustrated in Fig. 1 and formalized in Theorem 3.

Theorem 3. Let \mathbf{A}_τ denote the extended data matrix of available state samples at discrete time τ , \mathbf{Y}_τ the corresponding safety label matrix, and $B_\tau(\mathbf{x})$ the learned CBF. Suppose that ΔN new state samples are observed at time $\tau + 1$, with extended data matrix $\Delta \mathbf{A}$ and label matrix $\Delta \mathbf{Y}$. Then the updated CBF satisfies

$$B_{\tau+1}(\mathbf{x}) = B_\tau(\mathbf{x}) + 2\tilde{\mathbf{x}}^\top (\mathbf{K}_\tau \Delta \mathbf{Q} - \Delta \mathbf{K} \mathbf{Q}_\tau - \Delta \mathbf{K} \Delta \mathbf{Q}) \begin{bmatrix} 0 \\ 1 \end{bmatrix}, \quad (38)$$

where

$$\begin{cases} \mathbf{K}_\tau = (\lambda \mathbf{I} + \mathbf{A}_\tau^\top \mathbf{A}_\tau)^{-1}, \\ \mathbf{Q}_\tau = \mathbf{A}_\tau^\top \mathbf{Y}_\tau - \mathbf{A}_\tau^\top \mathbf{Y}_\tau \mathbf{C}, \\ \Delta \mathbf{K} = \mathbf{K}_\tau \Delta \mathbf{A}^\top (\mathbf{I} + \Delta \mathbf{A} \mathbf{K}_\tau \Delta \mathbf{A}^\top)^{-1} \Delta \mathbf{A} \mathbf{K}_\tau, \\ \Delta \mathbf{Q} = \Delta \mathbf{A}^\top \Delta \mathbf{Y} - \Delta \mathbf{A}^\top \Delta \mathbf{Y} \mathbf{C}. \end{cases} \quad (39)$$

Proof At time $\tau + 1$, the augmented data and label matrices are given by

$$\mathbf{A}_{\tau+1} = \begin{bmatrix} \mathbf{A}_\tau \\ \Delta \mathbf{A} \end{bmatrix}, \quad \mathbf{Y}_{\tau+1} = \begin{bmatrix} \mathbf{Y}_\tau \\ \Delta \mathbf{Y} \end{bmatrix}. \quad (40)$$

According to Eq. (13) and (40), the updated weight matrix can be written as

$$\mathbf{W}_{b,\tau+1} = \mathbf{K}_{\tau+1} \cdot \mathbf{Q}_{\tau+1}, \quad (41)$$

where

$$\begin{aligned} \mathbf{K}_{\tau+1} &= (\lambda \mathbf{I} + \mathbf{A}_\tau^\top \mathbf{A}_\tau + \Delta \mathbf{A}^\top \Delta \mathbf{A})^{-1}, \\ \mathbf{Q}_{\tau+1} &= \mathbf{A}_\tau^\top \mathbf{Y}_\tau + \Delta \mathbf{A}^\top \Delta \mathbf{Y} - \mathbf{A}_\tau^\top \mathbf{Y}_\tau \mathbf{C} - \Delta \mathbf{A}^\top \Delta \mathbf{Y} \mathbf{C}. \end{aligned} \quad (42)$$

Using the Woodbury matrix identity [43], [44], $\mathbf{K}_{\tau+1}$ and $\mathbf{Q}_{\tau+1}$ admit the incremental forms

$$\begin{aligned} \mathbf{K}_{\tau+1} &= \mathbf{K}_\tau - \Delta \mathbf{K}, \\ \mathbf{Q}_{\tau+1} &= \mathbf{Q}_\tau + \Delta \mathbf{Q}, \end{aligned} \quad (43)$$

where

$$\begin{aligned} \Delta \mathbf{K} &= \mathbf{K}_\tau \Delta \mathbf{A}^\top (\mathbf{I} + \Delta \mathbf{A} \mathbf{K}_\tau \Delta \mathbf{A}^\top)^{-1} \Delta \mathbf{A} \mathbf{K}_\tau, \\ \Delta \mathbf{Q} &= \Delta \mathbf{A}^\top \Delta \mathbf{Y} - \Delta \mathbf{A}^\top \Delta \mathbf{Y} \mathbf{C}. \end{aligned} \quad (44)$$

Substituting Eq. (43) into Eq. (41) yields

$$\begin{aligned} \mathbf{W}_{b,\tau+1} &= (\mathbf{K}_\tau - \Delta \mathbf{K})(\mathbf{Q}_\tau + \Delta \mathbf{Q}) \\ &= \mathbf{W}_{b,\tau} + \mathbf{K}_\tau \Delta \mathbf{Q} - \Delta \mathbf{K} \mathbf{Q}_\tau - \Delta \mathbf{K} \Delta \mathbf{Q}. \end{aligned} \quad (45)$$

Finally, substituting into the CBF expression gives

$$\begin{aligned} B_{\tau+1}(\mathbf{x}) &= 2\tilde{\mathbf{x}}^\top \mathbf{W}_{b,\tau+1} [0, 1]^\top - 1 \\ &= B_\tau(\mathbf{x}) + 2\tilde{\mathbf{x}}^\top (\mathbf{K}_\tau \Delta \mathbf{Q} - \Delta \mathbf{K} \mathbf{Q}_\tau - \Delta \mathbf{K} \Delta \mathbf{Q}) [0, 1]^\top. \end{aligned} \quad (46)$$

Remark 2. Since $\Delta \mathbf{A} \mathbf{K}_\tau \Delta \mathbf{A}^\top$ is a square matrix whose dimension equals the number of newly observed state samples ΔN , the time complexity of computing the matrix inverse involved in $\Delta \mathbf{K}$ is on the order of $\mathcal{O}(\Delta N^3)$. In practice, ΔN is typically much smaller than the total number of state samples used during offline training. Consequently, the computational cost of incrementally updating the CBF is substantially lower than that of retraining the CBF from scratch using the entire dataset.

In addition to adapting to changes in the real unsafe region, SafeLink also supports efficient online adjustment of the misclassification parameter c_1 , providing an additional degree of flexibility in shaping the learned unsafe region.

Theorem 4. Let $\mathbf{W}_{b,\tau}$ denote the weight matrix at time τ , corresponding to the current misclassification cost c_1 . If the misclassification cost for all unsafe samples is increased by Δc_1 , then the updated weight matrix $\mathbf{W}'_{b,\tau}$ is given by

$$\mathbf{W}'_{b,\tau} = \mathbf{W}_{b,\tau} + \Delta c_1 \mathbf{K}_\tau \mathbf{A}_u^\top \mathbf{1}_u \begin{bmatrix} 0 \\ -1 \end{bmatrix}^\top, \quad (47)$$

where \mathbf{K}_τ is defined as in Theorem 3, \mathbf{A}_u is the submatrix of \mathbf{A}_τ corresponding to the unsafe training set \mathcal{X}_u , and $\mathbf{1}_u$ is an all-ones column vector of dimension $|\mathcal{X}_u|$.

Proof From Eq. (17), the weight matrix is $\mathbf{W}_{b,\tau} = \mathbf{K}_\tau \mathbf{Q}_\tau$, where $\mathbf{Q}_\tau = \mathbf{A}^\top (\mathbf{Y}_\tau - \mathbf{Y}_\tau \mathbf{C})$. Let the updated cost matrix be $\mathbf{C}' = \mathbf{C} + \Delta \mathbf{C}$, with $\Delta \mathbf{C} = \begin{bmatrix} 0 & \Delta c_1 \\ 0 & 0 \end{bmatrix}$. Then the updated \mathbf{Q}_τ is

$$\mathbf{Q}'_\tau = \mathbf{A}_\tau^\top (\mathbf{Y}_\tau - \mathbf{Y}_\tau \mathbf{C}') = \mathbf{Q}_\tau - \mathbf{A}_\tau^\top \mathbf{Y}_\tau \Delta \mathbf{C}. \quad (48)$$

For an unsafe sample $\mathbf{x}_i \in \mathcal{X}_u$, the corresponding row of \mathbf{Y}_τ is $\tilde{\mathbf{y}}_i^\top = [1, 0]$, yielding $\tilde{\mathbf{y}}_i^\top \Delta \mathbf{C} = [0, \Delta c_1]$. For a safe

sample $\mathbf{x}_j \in \mathcal{X}_s$, we have $\tilde{\mathbf{y}}_j^\top \Delta \mathbf{C} = [0, 0]$. Thus, $\mathbf{Y}_\tau \Delta \mathbf{C}$ has rows $[0, \Delta c_1]$ corresponding to \mathcal{X}_u and zeros elsewhere.

Substituting this into the expression for the updated weight matrix, we obtain

$$\begin{aligned} \mathbf{W}'_{b,\tau} &= \mathbf{K}_\tau (\mathbf{Q}_\tau - \mathbf{A}_u^\top \mathbf{1}_u [0 \ \Delta c_1]) \\ &= \mathbf{W}_{b,\tau} + \Delta c_1 \mathbf{K}_\tau \mathbf{A}_u^\top \mathbf{1}_u [0 \ -1], \end{aligned} \quad (49)$$

which completes the proof. \blacksquare

Remark 3. In dynamic environments where the CBF $B_\tau(\mathbf{x})$ is updated at discrete times, the sudden appearance of new unsafe regions may temporarily place the system state $\mathbf{x}(t)$ outside the updated safe set, even if it was within the safe set in the previous interval. To ensure safety across all time segments, the Class- \mathcal{K} function $\alpha_i(\cdot)$ can be adaptively increased. By selecting a sufficiently large gain for α_i , the controller enforces a larger safety margin relative to the previous boundary and accelerates convergence back to the safe manifold if a violation occurs after an update. This adaptive tuning guarantees continuous collision avoidance despite the piecewise-constant switching of the learned CBF.

Algorithm 1: SafeLink Framework

Input: System dynamics $\dot{\mathbf{x}} = \mathbf{f}(\mathbf{x}) + \mathbf{g}(\mathbf{x})\mathbf{u}$, offline state points $\{\mathbf{x}_i\}_{i=1}^N$ with safety labels, cost matrix \mathbf{C} , regularization parameter λ , initial state \mathbf{x}_0 , target state \mathbf{x}_e , allowed error ϵ .

- 1 **Offline stage:**
 - 2 Initialize \mathbf{W}_e and \mathbf{b}_e in Eq. (10) randomly
 - 3 Compute \mathbf{A}_τ and \mathbf{Y}_τ according to Eq. (11)
 - 4 Derive \mathbf{K}_τ , \mathbf{Q}_τ , and $\mathbf{W}_{b,\tau}$ via Eq. (17)
 - 5 Construct the CBF $B_\tau(\mathbf{x})$ as in Eq. (19)
 - 6 Set current state $\mathbf{x}_t \leftarrow \mathbf{x}_0$
 - 7 **Control stage:**
 - 8 **while** $\|\mathbf{x}_e - \mathbf{x}_t\|_2 > \epsilon$ **do**
 - 9 Determine reference input \mathbf{u}_r using optimal control theory (without safety constraints)
 - 10 Compute $L_f^r B$ and $L_g L_f^{r-1} B$ as in Eqs. (20) and (21)
 - 11 Solve Eq. (9) to obtain safe control input \mathbf{u}_{safe}
 - 12 Update state via $\dot{\mathbf{x}} = \mathbf{f}(\mathbf{x}) + \mathbf{g}(\mathbf{x})\mathbf{u}_{safe}$
 - 13 **if** Unsafe region has changed **then**
 - 14 Collect newly observed state points with safety labels
 - 15 Compute $\Delta \mathbf{A}$ and $\Delta \mathbf{Y}$ via Eqs. (10) and (11)
 - 16 Update $B_\tau(\mathbf{x})$, \mathbf{K}_τ , \mathbf{Q}_τ , and $\mathbf{W}_{b,\tau}$ according to Theorem 3
 - 17 **end**
 - 18 **end**
-

The SafeLink procedure is summarized in Algorithm 1, which operates in three stages. In the offline stage, the CBF $B_\tau(\mathbf{x})$ is constructed using the training dataset, as detailed in lines 1–5. During the control stage, the reference input \mathbf{u}_r and the Lie derivatives of $B_\tau(\mathbf{x})$ are used to compute the safe control input \mathbf{u}_{safe} and update the system state, as shown in lines 7–12. Finally, if the unsafe region evolves over

time, newly observed state points and their safety labels are collected, and $B_\tau(\mathbf{x})$ is incrementally updated according to Theorem 3.

IV. EXPERIMENTS

In this section, the effectiveness of SafeLink is validated on a two-link manipulator, demonstrating its capability to simultaneously reach a target and avoid collisions within irregular and dynamic unsafe regions. Furthermore, we conduct ablation studies and benchmarking of update efficiency against other machine learning-based approaches.

A. Settings

A second-order nonlinear endpoint control problem is considered for a two-link manipulator with its base fixed at the origin. The link lengths are $L_1 = L_2 = 4\text{m}$. The angle between the first link and the x -axis is denoted by θ_1 with angular velocity ω_1 , while the angle between the second link and the first link is denoted by θ_2 with angular velocity ω_2 . The system states and dynamics are defined as:

$$\begin{cases} \mathbf{z} = [\theta_1, \theta_2, \omega_1, \omega_2]^\top, \\ \dot{\mathbf{z}} = \begin{bmatrix} 0 & 0 & 1 & 0 \\ 0 & 0 & 0 & 1 \\ 0 & 0 & 0 & 0 \\ 0 & 0 & 0 & 0 \end{bmatrix} \begin{bmatrix} \theta_1 \\ \theta_2 \\ \omega_1 \\ \omega_2 \end{bmatrix} + \begin{bmatrix} 0 & 0 \\ 0 & 0 \\ 1 & 0 \\ 0 & 1 \end{bmatrix} \begin{bmatrix} u_1 \\ u_2 \end{bmatrix}, \\ x = L_1 \cos \theta_1 + L_2 \cos(\theta_1 + \theta_2), \\ y = L_1 \sin \theta_1 + L_2 \sin(\theta_1 + \theta_2), \end{cases} \quad (50)$$

where (x, y) denotes the endpoint position, and the control inputs are constrained as $u_1, u_2 \in [-2, 2] \text{ rad/s}^2$.

The RVFL is configured with $N_1 = N_2 = 10$, $\lambda = 0.001$, and cost-sensitivity parameter $c_2 = 1$. The activation function is chosen as $\phi(x) = \text{sigmoid}(5x)$, a twice-differentiable variant of the sigmoid function with Lipschitz-continuous derivatives of all orders. Both α_2 in Eq. (7) and α_1 in Eq. (5) are linear functions with unit coefficients. The prediction interval is fixed at $\Delta t = 0.05 \text{ s}$.

To illustrate the necessity of learning-based CBF construction, the manipulator is simulated in an environment containing stacked parts and cargo, forming a highly irregular unsafe region that is difficult to represent analytically. The unsafe region is defined as the union of multiple stacked rectangles (Fig. 2). In the offline stage, 5,000 state points are uniformly sampled within $x, y \in [-15, 15]$ and labeled according to safety: +1 for safe and -1 for unsafe points, as shown in Fig. 3. Since each $[\theta_1, \theta_2]$ uniquely determines $[x, y]$, but the inverse mapping is not unique, the model is trained using unsafe-region information in $[x, y]$ space. When computing CBF constraints, derivatives with respect to $[x, y]$ are converted to derivatives with respect to $[\theta_1, \theta_2, \omega_1, \omega_2]$ via the chain rule.

The system is initialized at $[x, y, \theta_1, \theta_2, \omega_1, \omega_2] = [0, 0, 0, 0, 0, 0]$, and the target endpoint position is set to $[x, y] = [-4.1, 6.9]$, within the singularity-free workspace. Simulations are performed in MATLAB on a platform with an Intel i5-13600KF CPU (14 cores, 3.50 GHz, 20 threads) and 32 GB of RAM.

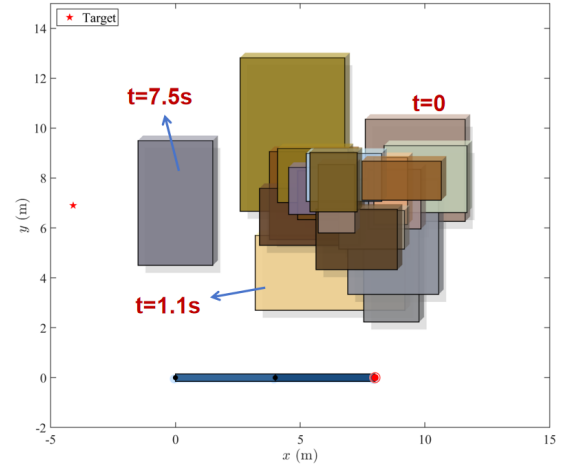


Fig. 2: Evolution of unsafe regions. The unsafe regions expand at $t = 1.1 \text{ s}$ and $t = 7.5 \text{ s}$.

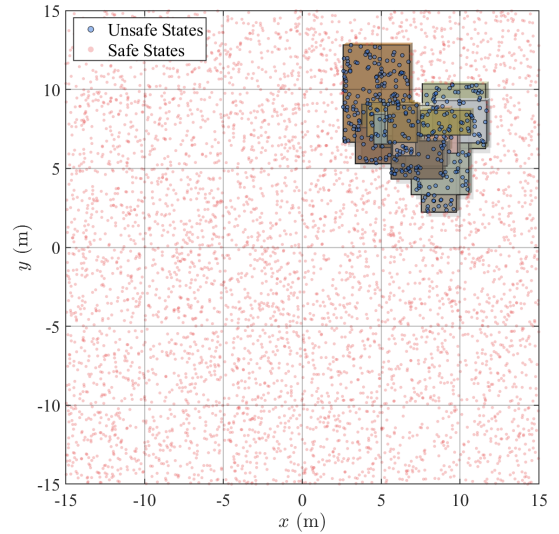


Fig. 3: Sampling in the state space. A total of 5000 state points are sampled.

B. Sensitivity Analysis of Misclassification Cost c_1

This section investigates the impact of the misclassification cost c_1 on the learned CBF, focusing on its influence on the classification bias between safe and unsafe regions. Table I summarizes the relationship between c_1 and the classification performance.

As observed, $N_{u \rightarrow s}$ monotonically decreases to zero as c_1 increases, which empirically validates the asymptotic safety properties formulated in Theorem 2. From a control perspective, the CBF functions as a conservative safety envelope that fully encloses all unsafe regions, ensuring that the system state remains within the safe set. A safety margin is simultaneously maintained to accommodate potential expansions of the unsafe region; accordingly, $c_1 = 2.0$ is selected.

C. Results

Model predictive control (MPC) is employed to generate reference control inputs [45], with the cost function defined

TABLE I: Performance of the learned CBF for different c_1 values.

c_1	0.5	1.0	1.1	1.2	1.3	1.4	1.5	2.0
$N_{u,s}$	22	3	3	2	2	1	0	0
$N_{s,u}$	56	94	96	106	113	118	132	178
<i>Accuracy</i>	99.22%	99.03%	99.01%	98.92%	98.86%	98.81%	98.68%	98.22%

*Notes: $N_{s \rightarrow u}$ represents the number of safe samples identified as unsafe, and $N_{u \rightarrow s}$ represents the number of unsafe samples identified as safe. *Accuracy* represents the ratio of correctly identified samples.

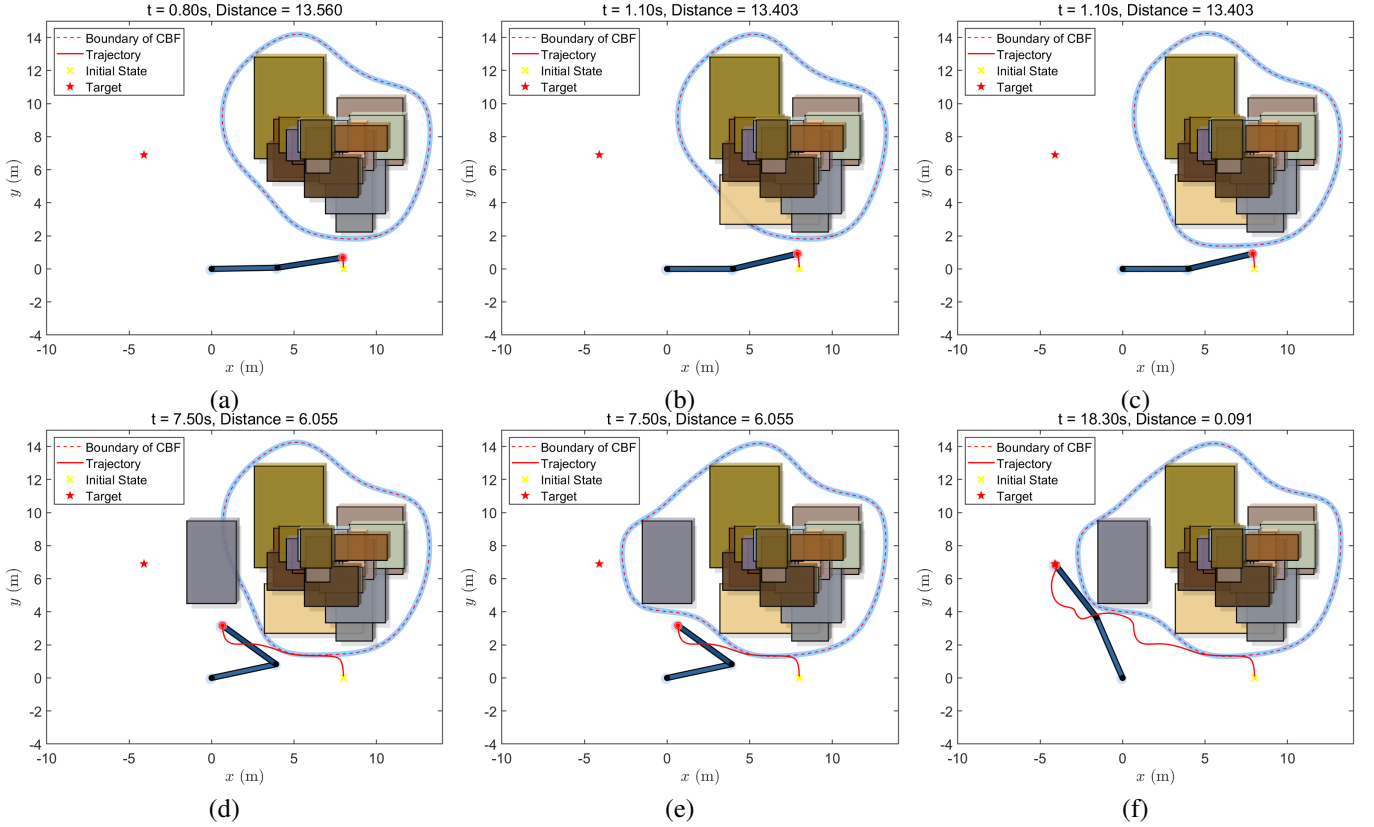


Fig. 4: Endpoint trajectories at different stages: (a) before the first environmental change, (b) after the first change, (c) after the first SafeLink update, (d) after the second change, (e) after the second SafeLink update, and (f) upon reaching the target state.

as

$$J = \sum_{k=1}^T \|\mathbf{p}_k - \mathbf{p}_{\text{target}}\|^2 + 0.01 \sum_{k=1}^T \|\mathbf{u}_k\|^2 + 10 \|\mathbf{p}_{T+1} - \mathbf{p}_{\text{target}}\|^2, \quad (51)$$

where $T = 20$ denotes the prediction horizon, and \mathbf{p}_k and $\mathbf{p}_{\text{target}}$ represent the current and target endpoint positions, respectively.

The unsafe region expands twice during the simulation: first at $t = 1.1s$, and again at $t = 7.5s$, as shown in Fig. 2. After each expansion, 100 state points within the newly added unsafe region are collected to update the CBF. To further enhance safety, the angular velocities ω_1 and ω_2 are constrained to $[-0.5 \text{ rad/s}, 0.5 \text{ rad/s}]$, which can also be enforced using CBFs.

Constraints on all angular velocities are expressed as

$$\begin{bmatrix} 0 & 0 & 1 & 0 \\ 0 & 0 & -1 & 0 \\ 0 & 0 & 0 & 1 \\ 0 & 0 & 0 & -1 \end{bmatrix} \mathbf{g}(z) \cdot \mathbf{u} \leq \begin{bmatrix} 0.5 - \omega_1 \\ 0.5 + \omega_1 \\ 0.5 - \omega_2 \\ 0.5 + \omega_2 \end{bmatrix}. \quad (52)$$

The final safe control input \mathbf{u}_{safe} is obtained by solving the QP in Eq. (9) subject to the constraints in Eq. (52). As shown in Fig. 5, the control inputs remain within the prescribed safety bounds of $[-2, 2] \text{ rad/s}^2$ and exhibit Lipschitz continuity during periods of region changes. The resulting endpoint trajectory is illustrated in Fig. 4. These results indicate that the CBF rapidly adapts to changes in the unsafe region, with its boundary effectively expanding to enclose newly added unsafe samples, thereby ensuring system safety.

For comparison, Fig. 6 presents the system trajectories under three scenarios: the reference method (MPC without obstacle consideration), SafeLink without CBF updates, and SafeLink without the cost-sensitive method. Specifically, the reference MPC approach focuses solely on path optimality, leading it to directly traverse unsafe regions. SafeLink without CBF updates remains outside the unsafe region for $t < 1.1s$; however, when the unsafe region expands at $t = 1.1s$ and $t = 7.5s$, the absence of an update mechanism causes the trajectory to enter the unsafe region during both intervals.

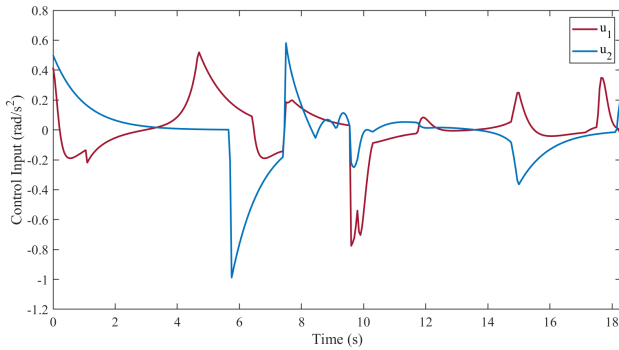


Fig. 5: Time evolution of the safe control inputs u_1 and u_2 .

For SafeLink without cost-sensitive learning, the learned CBF boundary partially approximates the unsafe region but fails to fully enclose it. Consequently, although the trajectory may remain outside the CBF boundary, collisions with the true unsafe region still occur. In contrast, the proposed method consistently avoids collisions in all these cases, demonstrating its effectiveness under dynamically evolving safety constraints.

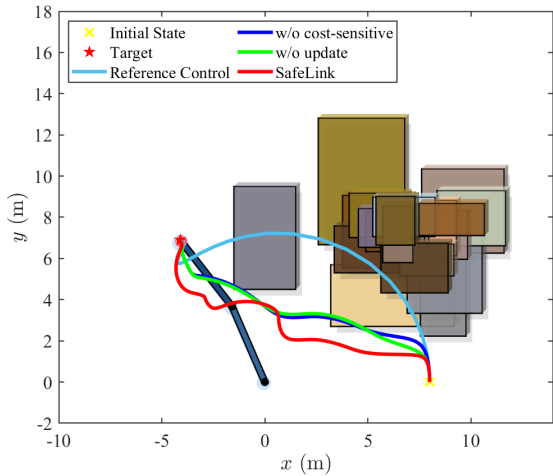


Fig. 6: Trajectories of the endpoint, where “w/o” denotes the absence of a specific part.

D. Update Efficiency Comparison

Finally, the training and update runtimes of SafeLink are compared with those of an SVM-based CBF [31] and an MLP-based CBF [33]. The SVM employs a Gaussian kernel with parameter-adaptive computation under the default MATLAB settings, while the MLP consists of three hidden layers with 10 neurons each. To isolate differences in temporal performance, the model capacities are adjusted to achieve comparable classification accuracies while ensuring that no unsafe state points are misclassified. Specifically, SafeLink is configured with $N_1 = 30$ and $N_2 = 30$.

Each method is trained and incrementally updated using the same dataset, and the results are summarized in Fig. 7. Notably, SafeLink exhibits a clear advantage in update efficiency, which becomes increasingly evident for complex systems with

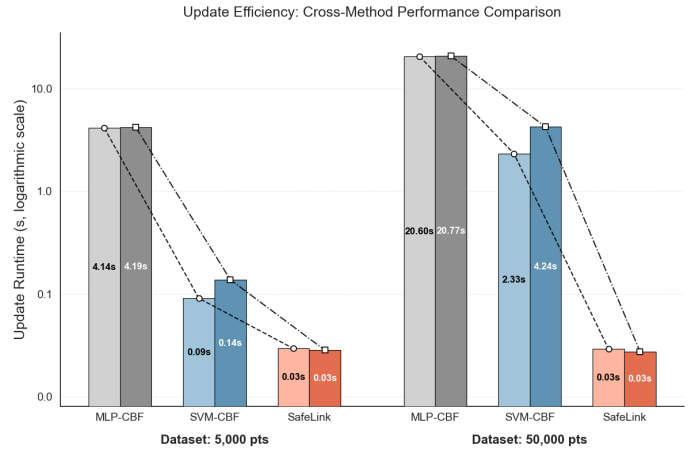


Fig. 7: Comparison of update efficiency across different methods and dataset scales. The bar chart (on a log scale) illustrates the updating runtime for MLP-CBF, SVM-CBF, and SafeLink under two dataset sizes (5,000 and 50,000 points).

larger offline training datasets. To further highlight this property, the size of the offline dataset is increased to 50,000 state points, and the experiments are repeated, as reported in Fig. 7. The results demonstrate that SafeLink achieves substantially lower update runtimes, particularly for large offline datasets, making it well suited for real-time control applications in dynamically changing environments.

V. CONCLUSION

In this paper, we have proposed a novel framework, termed SafeLink, which employs a cost-sensitive incremental RVFL to construct control barrier functions for safety-critical control. By incorporating a cost-sensitive term into the objective function of the RVFL, the boundary of the constructed CBF is able to conservatively enclose the unsafe regions, thereby ensuring the safety of the system. Safety properties of the identification process and incremental update theorems for the constructed CBF have been established, enabling real-time adaptation in dynamic unsafe regions. Experimental results on a nonlinear two-link manipulator have demonstrated the effectiveness of the proposed approach in enforcing safety constraints while supporting efficient real-time updates. In the future, several extensions can be pursued to enhance the proposed framework, such as deriving full-horizon safety guarantees across successive updates and extending its applicability to moving or multiple disconnected unsafe regions. In addition, it is also meaningful to integrate with reinforcement learning or adaptive MPC frameworks to adaptively tune the reference control input or the CBF parameters for better performance.

REFERENCES

- [1] Z. Liu, S. Hu, and X. He, “Real-time safety assessment of dynamic systems in non-stationary environments: A review of methods and techniques,” in *2023 CAA Symposium on Fault Detection, Supervision and Safety for Technical Processes (SAFEPROCESS)*, pp. 1–6, IEEE, 2023.
- [2] Z. Liu, X. He, B. Huang, and D. Zhou, “Incremental learning-enabled fault diagnosis of dynamic systems: A comprehensive review,” *IEEE Transactions on Cybernetics*, vol. 55, no. 12, pp. 5633–5649, 2025.

- [3] Y. Zhang, L. Wen, Z. Bing, X. Yao, L. Kong, W. He, and A. Knoll, "Adaptive safety-critical control for high-order systems: A real-time gaussian process approach," *IEEE Transactions on Automation Science and Engineering*, 2025.
- [4] J. Palmieri, P. Di Lillo, M. Lippi, S. Chiaverini, and A. Marino, "A control architecture for safe trajectory generation in human-robot collaborative settings," *IEEE Transactions on Automation Science and Engineering*, vol. 22, pp. 365–380, 2024.
- [5] S. Liu, Y. Mao, and C. A. Belta, "Safety-critical planning and control for dynamic obstacle avoidance using control barrier functions," in *2025 American Control Conference (ACC)*, pp. 348–354, IEEE, 2025.
- [6] A. Alan, A. J. Taylor, C. R. He, A. D. Ames, and G. Orosz, "Control barrier functions and input-to-state safety with application to automated vehicles," *IEEE Transactions on Control Systems Technology*, vol. 31, no. 6, pp. 2744–2759, 2023.
- [7] P. Han, Z. Liu, X. He, S. X. Ding, and D. Zhou, "Multi-condition fault diagnosis of dynamic systems: A survey, insights, and prospects," *IEEE Transactions on Automation Science and Engineering*, vol. 22, pp. 15728–15744, 2025.
- [8] B. Lacevic, P. Rocco, and A. M. Zanchettin, "Safety assessment and control of robotic manipulators using danger field," *IEEE Transactions on Robotics*, vol. 29, no. 5, pp. 1257–1270, 2013.
- [9] F. Blanchini, "Set invariance in control," *Automatica*, vol. 35, no. 11, pp. 1747–1767, 1999.
- [10] A. Clark, Z. Li, and H. Zhang, "Control barrier functions for safe cps under sensor faults and attacks," in *2020 59th IEEE Conference on Decision and Control (CDC)*, pp. 796–803, Ieee, 2020.
- [11] A. D. Ames, X. Xu, J. W. Grizzle, and P. Tabuada, "Control barrier function based quadratic programs for safety critical systems," *IEEE Transactions on Automatic Control*, vol. 62, no. 8, pp. 3861–3876, 2016.
- [12] A. D. Ames, S. Coogan, M. Egerstedt, G. Notomista, K. Sreenath, and P. Tabuada, "Control barrier functions: Theory and applications," in *2019 18th European control conference (ECC)*, pp. 3420–3431, IEEE, 2019.
- [13] C. Dawson, S. Gao, and C. Fan, "Safe control with learned certificates: A survey of neural lyapunov, barrier, and contraction methods for robotics and control," *IEEE Transactions on Robotics*, vol. 39, no. 3, pp. 1749–1767, 2023.
- [14] K. P. Tee, S. S. Ge, and E. H. Tay, "Barrier lyapunov functions for the control of output-constrained nonlinear systems," *Automatica*, vol. 45, no. 4, pp. 918–927, 2009.
- [15] S. Prajna and A. Jadbabaie, "Safety verification of hybrid systems using barrier certificates," in *International Workshop on Hybrid Systems: Computation and Control*, pp. 477–492, Springer, 2004.
- [16] J. Wang, W. Ren, W. Xia, and X.-M. Sun, "Control barrier functions for safe stabilization via zubov's theorem," *IEEE Transactions on Automation Science and Engineering*, vol. 23, pp. 1905–1916, 2026.
- [17] Y. Xiong, D.-H. Zhai, and Y. Xia, "Robust whole-body safety-critical control for sampled-data robotic manipulators via control barrier functions," *IEEE Transactions on Automation Science and Engineering*, 2025.
- [18] W. Xiao, T.-H. Wang, R. Hasani, M. Chahine, A. Amini, X. Li, and D. Rus, "Barriernet: Differentiable control barrier functions for learning of safe robot control," *IEEE Transactions on Robotics*, vol. 39, no. 3, pp. 2289–2307, 2023.
- [19] H.-g. Kang and Y. Kim, "Control barrier function based terrain and path following control of unmanned aerial vehicle considering attitude constraint," *The Aeronautical Journal*, vol. 129, no. 1337, pp. 1960–1981, 2025.
- [20] J. Breeden and D. Panagou, "Robust control barrier functions under high relative degree and input constraints for satellite trajectories," *Automatica*, vol. 155, p. 111109, 2023.
- [21] J. Huang, J. Zeng, X. Chi, K. Sreenath, Z. Liu, and H. Su, "Dynamic collision avoidance using velocity obstacle-based control barrier functions," *IEEE Transactions on Control Systems Technology*, 2025.
- [22] M. Rauscher, M. Kimmel, and S. Hirche, "Constrained robot control using control barrier functions," in *2016 IEEE/RSJ International Conference on Intelligent Robots and Systems (IROS)*, pp. 279–285, IEEE, 2016.
- [23] J. Sun, J. Yang, and Z. Zeng, "Safety-critical control with control barrier function based on disturbance observer," *IEEE Transactions on Automatic Control*, vol. 69, no. 7, pp. 4750–4756, 2024.
- [24] J. Xie, L. Hu, Y. Tan, and J. Yang, "Cbf-based hierarchical quadratic programs with guaranteed feasibility for safety-critical systems," *IEEE Transactions on Automation Science and Engineering*, vol. 22, pp. 23687–23699, 2025.
- [25] K. Zhao and Y. Song, "Decision function-based adaptive control of uncertain systems subject to irregular output constraints," *IEEE Transactions on Automatic Control*, 2024.
- [26] M. Gong, L. Sheng, and D. Zhou, "Robust fault-tolerant stabilisation of uncertain high-order fully actuated systems with actuator faults," *International Journal of Systems Science*, vol. 55, no. 12, pp. 2518–2530, 2024.
- [27] C. Li, Y. Liu, M. Gao, and L. Sheng, "Fault-tolerant formation consensus control for time-varying multi-agent systems with stochastic communication protocol," *International Journal of Network Dynamics and Intelligence*, pp. 100004–100004, 2024.
- [28] R. Cheng, G. Orosz, R. M. Murray, and J. W. Burdick, "End-to-end safe reinforcement learning through barrier functions for safety-critical continuous control tasks," in *Proceedings of the AAAI conference on artificial intelligence*, vol. 33, pp. 3387–3395, 2019.
- [29] M. Guerrier, H. Fouad, and G. Beltrame, "Learning control barrier functions and their application in reinforcement learning: A survey," *arXiv preprint arXiv:2404.16879*, 2024.
- [30] C. Dawson, Z. Qin, S. Gao, and C. Fan, "Safe nonlinear control using robust neural lyapunov-barrier functions," in *Conference on Robot Learning*, pp. 1724–1735, PMLR, 2022.
- [31] M. Srinivasan, A. Dabholkar, S. Coogan, and P. A. Vela, "Synthesis of control barrier functions using a supervised machine learning approach," in *2020 IEEE/RSJ International Conference on Intelligent Robots and Systems (IROS)*, pp. 7139–7145, IEEE, 2020.
- [32] W. Xiao, C. G. Cassandras, and C. A. Belta, "Learning feasibility constraints for control barrier functions," in *2023 European Control Conference (ECC)*, pp. 1–6, IEEE, 2023.
- [33] A. Robey, H. Hu, L. Lindemann, H. Zhang, D. V. Dimarogonas, S. Tu, and N. Matni, "Learning control barrier functions from expert demonstrations," in *2020 59th IEEE Conference on Decision and Control (CDC)*, pp. 3717–3724, IEEE, 2020.
- [34] S. Chen, Z. Wu, and P. D. Christofides, "Machine-learning-based construction of barrier functions and models for safe model predictive control," *AIChE Journal*, vol. 68, no. 6, p. e17456, 2022.
- [35] H. Zhang, J. Wu, Y. Vorobeychik, and A. Clark, "Exact verification of relu neural control barrier functions," *Advances in neural information processing systems*, vol. 36, pp. 5685–5705, 2023.
- [36] Z. Liu and X. He, "Online dynamic hybrid broad learning system for real-time safety assessment of dynamic systems," *IEEE Transactions on Knowledge and Data Engineering*, vol. 36, no. 12, pp. 8928–8938, 2024.
- [37] Y.-H. Pao, G.-H. Park, and D. J. Sobajic, "Learning and generalization characteristics of the random vector functional-link net," *Neurocomputing*, vol. 6, no. 2, pp. 163–180, 1994.
- [38] B. Igel'nik and Y.-H. Pao, "Stochastic choice of basis functions in adaptive function approximation and the functional-link net," *IEEE transactions on Neural Networks*, vol. 6, no. 6, pp. 1320–1329, 1995.
- [39] D. Needell, A. A. Nelson, R. Saab, P. Salanevich, and O. Schavemaker, "Random vector functional link networks for function approximation on manifolds," *Frontiers in Applied Mathematics and Statistics*, vol. 10, p. 1284706, 2024.
- [40] A. D. Ames, J. W. Grizzle, and P. Tabuada, "Control barrier function based quadratic programs with application to adaptive cruise control," in *53rd IEEE conference on decision and control*, pp. 6271–6278, IEEE, 2014.
- [41] W. Xiao and C. Belta, "High-order control barrier functions," *IEEE Transactions on Automatic Control*, vol. 67, no. 7, pp. 3655–3662, 2021.
- [42] Z. Liu and X. He, "Dynamic submodular-based learning strategy in imbalanced drifting streams for real-time safety assessment in non-stationary environments," *IEEE Transactions on Neural Networks and Learning Systems*, vol. 35, no. 3, pp. 3038–3051, 2024.
- [43] W. W. Hager, "Updating the inverse of a matrix," *SIAM review*, vol. 31, no. 2, pp. 221–239, 1989.
- [44] W. Li, Z. Liu, P. Han, X. He, L. Wang, and T. Zhang, "A dynamic anchor-based online semi-supervised learning approach for fault diagnosis under variable operating conditions," *Neurocomputing*, vol. 638, p. 130137, 2025.
- [45] H. Gao, Z. Chen, and W. Tang, "Trajectory tracking control of a flexible air-breathing hypersonic vehicle using lyapunov-based model predictive control," *Systems Science & Control Engineering*, vol. 12, no. 1, p. 2364035, 2024.